

RESEARCH ARTICLE

The diagnostic and prognostic value of tau-PET in amnesic MCI with different FDG-PET subtypes

Cecilia Boccalini^{1,2} , Silvia Paola Caminiti^{1,3,4} , Arturo Chiti^{1,4}, Giovanni B. Frisoni^{5,6},
Valentina Garibotto^{2,7,8}, Daniela Perani^{1,4}  & the Alzheimer's Disease Neuroimaging Initiative*

¹Vita-Salute San Raffaele University, Milan, Italy

²Laboratory of Neuroimaging and Innovative Molecular Tracers (NIMTlab), Geneva University Neurocenter and Faculty of Medicine, University of Geneva, Geneva, Switzerland

³Department of Brain and Behavioral Sciences, University of Pavia, Pavia, Italy

⁴Nuclear Medicine Department, IRCCS San Raffaele Scientific Institute, Milan, Italy

⁵Laboratory of Neuroimaging of Aging (LANVIE), University of Geneva, Geneva, Switzerland

⁶Memory Clinic, Geneva University Hospitals, Geneva, Switzerland

⁷Division of Nuclear Medicine and Molecular Imaging, Geneva University Hospitals, Geneva, Switzerland

⁸CIBM Center for Biomedical Imaging, Geneva, Switzerland

Correspondence

Daniela Perani, Division of Neuroscience, San Raffaele Scientific Institute Nuclear Medicine Unit, Vita-Salute San Raffaele University, San Raffaele Hospital, Via Olgettina 60, Milan 20132, Italy. Tel: (+39) 02.2643.2224; Fax: +39-02-26432717. E-mail: perani.daniela@hsr.it

Received: 25 January 2024; Revised: 21 February 2024; Accepted: 26 February 2024

Annals of Clinical and Translational Neurology 2024; 11(5): 1236–1249

doi: 10.1002/acn3.52039

*Data used in preparation of this article were also obtained from the Alzheimer's Disease Neuroimaging Initiative (ADNI) database (adni.loni.usc.edu). As such, the investigators within the ADNI contributed to the design and implementation of ADNI and/or provided data but did not participate in analysis or writing of this report. A complete listing of ADNI investigators can be found at: http://adni.loni.usc.edu/wpcontent/uploads/how_to_apply/ADNI_Acknowledgement_List.pdf.

Abstract

Objectives: Mild cognitive impairment presenting with an amnesic syndrome (aMCI) and amyloid positivity is considered due to AD. Many subjects, however, can show an overall very slow progression relevant for differential diagnosis, prognosis, and treatment. This study assessed PET biomarkers, including brain glucose metabolism, tau, and amyloid load, in a series of comparable aMCI at baseline, clinically evaluated at follow-up. **Methods:** We included 72 aMCI subjects from Geneva Memory Center ($N = 31$) and ADNI cohorts ($N = 41$), selected based on available FDG-PET, tau-PET, amyloid-PET, and clinical follow-up (2.3 years \pm 1.2). A data-driven algorithm classified brain metabolic patterns into subtypes that were then compared for clinical and PET biomarker measures and cognitive decline. Voxel-wise comparisons were performed both with FDG-PET and tau-PET data. **Results:** The algorithm classified three metabolic subtypes, namely “Hippocampal-sparing with cortical hypometabolism” (Type1; $N = 27$), “Hippocampal and cortical hypometabolism” (Type 2; $N = 23$), and “Medial temporal hypometabolism” (Type 3; $N = 22$). Amyloid positivity and tau accumulation in the medial temporal and neocortical regions characterized Type 1 and Type 2, whereas Type 3 showed no significant tau pathology, variable amyloid positivity, and stability at follow-up. All tau-positive patients, independently of the FDG-based subtype, showed faster cognitive decline. **Interpretation:** aMCI subjects can differ in metabolic patterns, tau and amyloid pathology, and clinical progression. Here, we complemented with PET tau biomarker the specific brain hypometabolic patterns at the individual level in the prodromal phase, contributing to the patient's classification. Tau PET is the most accurate biomarker in supporting or excluding the AD diagnosis in aMCI across metabolic subtypes and also predicting the risk of decline.

Introduction

Mild cognitive impairment (MCI) represents a heterogeneous clinical condition, in which the interaction of multiple pathogenic mechanisms and risk factors ultimately

leads to distinct clinical manifestations and outcomes. MCI subjects may convert to Alzheimer's disease (AD) and other neurodegenerative dementias, otherwise, they can remain stable or even revert to normal cognition.¹ Previous evidence showed the existence of individuals

with amnesic MCI (aMCI) condition older (typically around 75) and with an overall slow disease course. Pathological studies linked these features to limbic-predominant age-related TDP-43 encephalopathy (LATE), either with or without hippocampal sclerosis.² LATE has been associated with a progressive amnesic syndrome that can mimic AD clinical syndrome. The differentiation between LATE and AD is possible only postmortem as no validated in vivo biomarkers specific for TDP-43 pathology exist that would allow the detection of LATE neuropathological changes.

In AD, neuropathology and neuroimaging studies have consistently identified three subtypes^{3–5}: the “hippocampal-sparing” subtype, characterized by atrophy, extensive cortical glucose hypometabolism, and in vivo and postmortem evidence of extensive neurofibrillary tau tangles (NFT) in the associative cortex, with a malignant AD clinical phenotype; the “Typical AD” subtype characterized by atrophy, hypometabolism, and NFT involving both the medial temporal structures and associative cortices; and the “limbic” subtype characterized by atrophy, hypometabolism, and high NFT only in the MTL, with low cerebrospinal fluid (CSF) tau levels, older age at onset, and slow clinical progression. Although all these subtypes are usually attributed to AD,^{3–5} the limbic subtype characterized by a hypometabolism in medial temporal structures, strikingly resembles the pattern described in pathologically confirmed patients with LATE pathology,⁶ thus, leading to an uncertain diagnosis.^{3,4} Moreover, the limbic-predominant pattern has been associated with the presence of TDP-43 pathology at postmortem.⁷ Limbic-predominant hypometabolism pattern was also associated with clinical stability in aMCI, hampering progression to AD.⁸ However, given the borderline distinction between limbic-predominant AD and patients with LATE pathology, biomarkers able to discriminate would be of great relevance, especially in the prodromal phases. Despite the increasingly validated role of tau-PET,^{9,10} only one case study¹¹ focused specifically on the contribution of tau-PET in differentiating between non-AD and AD subtypes in a homogeneous AD-mimicking amnesic population in the prodromal disease stage. We hypothesized that independent of the brain hypometabolic patterns, the presence of diffuse tau pathology could support AD diagnosis and predict cognitive decline. On the other hand, a negative tau-PET result would confirm a non-AD neurodegenerative etiology in aMCI subjects.

This study aims to capture the possible brain metabolic heterogeneity during the aMCI prodromal phase by applying a data-driven algorithm based on FDG-PET¹² to define hypometabolism-based subtypes in clinically comparable aMCI subjects, and subsequently compare them in terms of tau and amyloid biomarkers assessed by PET,

and clinical follow-up. This classification could usefully inform subject selection in disease-modifying treatments.

Methods

Participants

Subjects with aMCI were retrospectively included from the memory center of Geneva University Hospitals (HUG), and the Alzheimer’s Disease Neuroimaging Initiative (ADNI) database, screening the ADNI-3 phase with tau PET available. ADNI is a US public-private partnership launched in 2003 and led by Principal Investigator Michael W. Weiner, MD. The primary goal of ADNI has been to collect data on MCI subjects and AD patients, as well as on healthy controls, evaluating the combined prognostic value of several AD biomarkers and clinical and neuropsychological assessments. For up-to-date information, see <https://adni.loni.usc.edu>.

We applied strict inclusion criteria for our sample: (i) aMCI diagnosis according to Petersen criteria¹; (ii) Mini-Mental State Examination (MMSE), (iii) an FDG-PET scan performed at baseline and analyzed using the optimized SPM procedure¹³ showing brain hypometabolism in the typical AD-like structures, namely the hippocampal structures and/or the temporoparietal associative cortex¹² (iv) a tau-PET scan and (v) a structural MRI, both within a year from FDG-PET. Thus, subjects with completely negative FDG-PET scans or non-AD FDG-PET hypometabolic features were excluded. Other exclusion criteria were (i) presence of neoplastic or significant cerebrovascular lesions; (ii) neurosurgery or other neurological conditions, including epilepsy, encephalitis, or stroke (iii) clinically relevant psychiatric disorders, in accordance with DSM-IV criteria; (iv) current or a recent history of drug or alcohol abuse/dependence.

Considering the above strict inclusion criteria, 31 and 41 aMCI subjects from the HUG memory clinic and ADNI cohorts, respectively, participated in the study, resulting in a final whole sample of 72 individuals. 48 out of 72 participants also underwent amyloid-PET within a year from FDG-PET and 57 out of 72 had a follow-up MMSE at 2.3 ± 1.2 years.

The local Ethics Committee approved the imaging studies, which have been conducted under the principles of the Declaration of Helsinki and the International Conference on Harmonization Good Clinical Practice. Each subject or their relatives provided voluntary written informed consent to participate in the studies.

Imaging acquisition and processing

Regarding aMCI subjects from the Geneva memory clinic, all PET scans using ¹⁸F-labeled tracers were performed at

the Nuclear Medicine and Molecular Imaging division at HUG with Biograph128mCT, Biograph128 Vision 600 Edge, Biograph40 mCT, or Biograph64 TruePoint PET scanners (Siemens Medical Solutions, Malvern, PA, USA). All scanners were thus from the same vendor and of the same generation, harmonized regarding their performance and reconstructions, and cross-calibrated. For all tracers, data were acquired in list mode and were reconstructed using 3D OSEM, corrected for randoms, dead time, normalization, scatter, attenuation, and sensitivity, and averaged after motion correction. A 2-mm Gaussian filter at full width at half maximum (FWHM) was applied resulting in images with 400×400 matrix with 1.01 mm isotropic voxels.

FDG-PET

FDG-PET acquisition at HUG was performed according to the European Association of Nuclear Medicine (EANM) guidelines.¹⁴ ADNI acquisition procedures are detailed in the “ADNI PET technical procedures manual, version 9.5” (<https://adni.loni.usc.edu/methods/pet-analysis-method/pet-analysis/>). Only the last three 5-min frames of FDG-PET images were retrieved from the database and combined to obtain a single 15-min static image. In such a way, we ensured uniform acquisition procedures for all FDG-PET images, independently of the acquisition site.¹⁵

A visual quality check of the images was performed to identify potential artifacts (e.g., acquisition issues and excessive patient motion) and issues related to technical characteristics, such as the use of compatible reconstruction algorithms. Then, all FDG-PET images were each normalized to the optimized FDG-PET template,¹⁶ using SPM12 (<https://www.fil.ion.ucl.ac.uk/spm/>). They were then scaled to the global mean of the activity within the brain and finally smoothed with an isotropic 3D Gaussian kernel (8 mm full-width half maximum), according to the validated pipeline proposed for our single-subject SPM-based analysis.¹³ This kind of smoothing is required for the random field theory to be applicable. It is also effective in reducing the number of multiple comparisons to be performed. Each FDG-PET single-subject scan was tested for brain hypometabolism by applying a two-sample *t*-test comparison with a validated FDG-PET database of healthy controls (HC; $N = 112$) on a voxel-by-voxel basis, including age as a covariate.¹³ The *p*-value of the single-subject hypometabolism maps was set at $p < 0.05$ uncorrected at cluster level, with a cluster-forming threshold of $n = 100$ voxels, based on previous literature.¹⁵ The SPM-based single-subject procedure has been demonstrated not to be affected by different scanners used for acquisitions.¹⁷ For subsequent statistical

comparisons, the SPM-t hypometabolism maps were converted into the normal *z*-like distribution (SPM-*z* maps) with MATLAB R2021b (Mathworks Inc., Sherborn, MA, USA). Low *z*-scores (<0) indicated more severe regional hypometabolism compared to HC. Moreover, REX toolbox (<https://www.nitrc.org/projects/rex/>) was used to extract the mean metabolism values from the hippocampus, entering as sources the scaled FDG-PET images of patients and HC.

Tau-PET

[¹⁸F] flortaucipir (¹⁸F-AV1451) was used for the tau-PET scans in both HUG and ADNI. Regarding HUG, the tracer was synthesized at the Center for Radiopharmaceutical Sciences in Villigen, Switzerland, under license from the intellectual property (IP) owner (Avid subsidiary of Lilly, Philadelphia, PA, USA). Subjects received 180 MBq of [¹⁸F]-AV1451, with image acquisition performed 75 min after injection (acquisition time 30 min). Each emission frame was reconstructed in 6×5 -min frames. ADNI sample followed a similar acquisition procedure according to ADNI 3 PET protocols (<https://adni.loni.usc.edu/methods/pet-analysis-method/pet-analysis/>) and the six 5-min frames were retrieved from the ADNI database and combined to obtain a single static image. For all scans, processing was performed using Statistical Parametric Mapping (SPM12, Wellcome Trust Centre for Neuroimaging, London, UK), running in MATLAB R2018b Version 9.5 (MathWorks Inc., Sherborn, MA, USA). MRI 3D T1 images were aligned to a reference plane passing through the anterior commissure, segmented into gray matter, white matter, and cerebrospinal fluid tissue compartments, and normalized to the Montreal Neurologic Institute (MNI) space using tissue probability maps. All PET images were aligned to the subject's respective T1 MRI scan and normalized to the MNI space using the transformation matrix that was generated during the registration of the MRI images to the standard space. Tau distribution was visually assessed by two expert nuclear medicine physicians (VG, DP), according to published recommendations,¹⁸ describing regions of increased [¹⁸F] flortaucipir uptake. Tau status was defined based on visual assessment, where negativity was defined as stage 0, MTL-limited as stages I–III, and positivity was defined as stages IV–VI.¹⁹ The standardized uptake values (SUVr) were calculated from the regions of interest (ROIs) of the automated anatomic labeling atlas 3,²⁰ using the cerebellar crus as a reference region. We also calculated the global SUVr from the entorhinal cortex, lateral occipital cortex, inferior temporal cortex, and amygdala.²¹ Intensity-normalized PET images were saved for voxel-wise analyses.

Amyloid-PET

Amyloid-PET images were acquired using [^{18}F] florbetapir (FBP) (HUG and ADNI), or [^{18}F] flutemetamol (FMM) (HUG) tracers. FBP late images were acquired 50 min after the intravenous administration of 210 ± 18 MBq (3×5 -min image frames). FMM late images were acquired 90 min after the intravenous administration of 166 ± 16 MBq (4×5 -min image frames). ADNI FBP images were acquired at 50–70 min post-injection of 370 MBq (10.1 mCi) $\pm 10\%$, (4×5 -min frames), according to ADNI protocols (<https://adni.loni.usc.edu/methods/pet-analysis-method/pet-analysis/>). Images were then averaged into a single 20-min frame. The same processing pipeline used for tau-PET images was applied to all amyloid-PET images. SUVR was calculated using the whole cerebellum as the reference region. SUVR was extracted from the Centiloid volume-of interest (VOI) and converted into Centiloid units as recommended by Klunk.²² A Centiloid value of 19 was used as the cutoff point to define amyloid positive versus negative individuals.²³ All amyloid-PET images were also visually assessed by two expert nuclear medicine physicians (V.G., D.P.) applying the standard operating procedures approved by the European Medicines Agency (https://www.ema.europa.eu/documents/product-information/vizamyl-epar-product_information_en.pdf; https://www.ema.europa.eu/documents/product-information/amyvid-epar-product_information_en.pdf) and classified into “A+” or “A–.”

FDG-PET subtypes classification

Classification of FDG-PET subtypes was performed according to a procedure recently validated in another large sample of aMCI.¹² Briefly, the procedure consists of a three-step classification algorithm that combines information from the typical AD-like and limbic-like patterns and related hallmark regions (HR). The patterns and HRs were constructed using the automated anatomical labeling atlas (AAL) of functional anatomical regions.²⁴ REX toolbox (<https://www.nitrc.org/projects/rex/>) was used to extract the number of hypometabolic voxels from AD-like and limbic patterns and HRs from single-subject SPM-z hypometabolic maps (see FDG-PET section).

In the first step, we counted the hypometabolic voxels within the AD-like and limbic-like patterns, and we binarily classified each individual. In the second step, we performed the same procedure for AD and limbic HR to obtain the HR classification. In the third step, we combined the pattern and HR classifications to identify the following subtypes: (1) “Hippocampal-sparing with

cortical hypometabolism” (Type 1) subtype with relatively high values of AD cortical pattern and HR; (2) “Hippocampal and cortical hypometabolism” (Type 2) subtype with relatively high values of both AD pattern and limbic HR or limbic pattern and AD HR; (3) “Medial temporal cortex hypometabolism” (Type 3) subtype with relatively high values of limbic pattern and HR.

Statistical analyses

Baseline demographics, clinical, cognitive, and biomarkers differences among FDG-PET subtypes were assessed using a Kruskal-Wallis rank sum test for continuous variables and a proportion test for categorical variables. Biomarkers differences were tested in terms of binary status and, also, tau and amyloid loads (global tau SUVR, tau SUVR in the hippocampus and in the inferior temporal gyrus, and centiloid). Differences in hippocampal metabolism were also tested. To investigate the cognitive trajectories of FDG-PET subtypes over time we applied linear mixed-effects models with random intercepts and slopes using longitudinal MMSE as a dependent variable, adjusting for age, sex, and education. We applied the same longitudinal model to examine differences in cognitive decline between groups stratified according to tau.

All analyses were performed using R, version 4.0.2 (<https://www.r-project.org/>). A p -value of 0.05 was considered the significance threshold for all analyses.

Voxel-wise analyses

A voxel-wise SPM t -test analysis was applied to compare each aMCI subtype with a set of HC subjects ($N = 112$) to assess brain metabolism at the group level. A voxel-wise analysis was applied to assess tau accumulation in each aMCI subtype compared to a pool of HC ($N = 43$, recruited from HUG and ADNI). Voxel-wise differences in metabolism and tau accumulation between subtypes were also tested. The statistical threshold was set at $p = 0.005$, FWE-corrected for multiple comparisons. Only clusters containing more than 100 voxels were deemed to be significant.

Results

FDG-PET subtypes

27 aMCI subjects were classified as “Hippocampal-sparing with cortical hypometabolism” Type 1; 23 aMCI as “Hippocampal and cortical hypometabolism” Type 2; 22 as “Medial temporal cortex hypometabolism” Type 3. Examples of individual cases are reported in Fig 1.

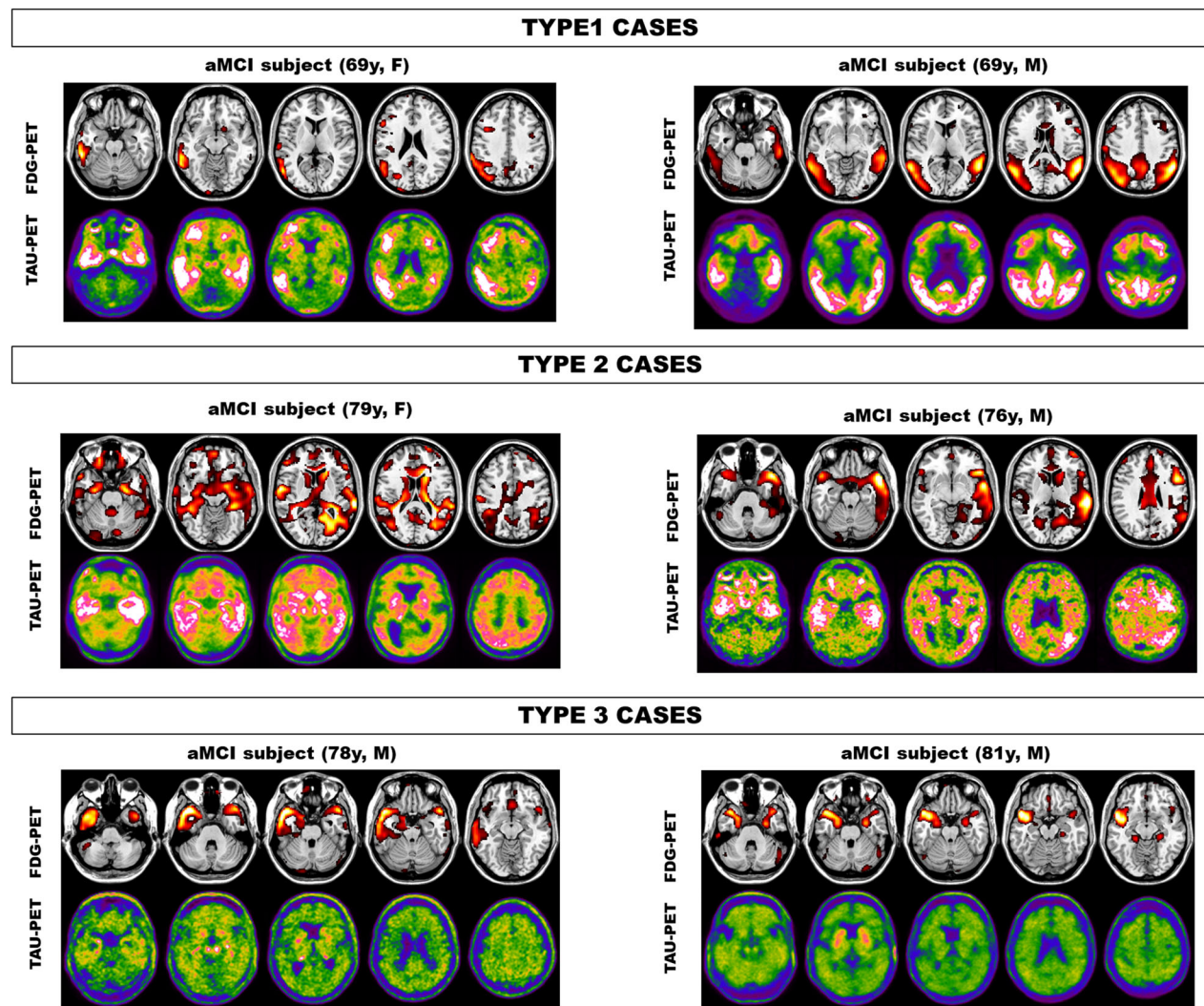


Figure 1. Individual examples of brain hypometabolic patterns and tau distribution for each subtype. The single-subject FDG-PET hypometabolic patterns resulted from statistical parametric mapping (SPM) single-subject analysis versus 112 controls; significance was set at uncorrected $p < 0.05$ at the voxel level with $k > 100$ voxels. Yellow/red scales represent hypometabolism severity ($p < 0.05$, $k = 100$). For tau-PET, SUVR images are displayed and green-to-pink scales represent tau load severity. Type 1 corresponds to the hippocampal-sparing subtype with cortical hypometabolism; Type 2 to the typical AD subtype with hippocampal and cortical hypometabolism; Type 3 to the limbic subtype with medial temporal cortex hypometabolism.

The three subtypes differed in global cognition and biomarkers' status, but not in other variables (Table 1). The patients with Type 1 and Type 2 were all amyloid- and tau-positive.

Type 3 showed significantly higher MMSE and MOCA scores compared to the other two subtypes ($p < 0.05$). A higher percentage of tau-negative including negative scans (78%) or MTL-limited (18%) and amyloid-negative (50%) individuals were found in Type 3 compared to the other groups ($p < 0.001$ and $p = 0.02$, respectively).

Differences in tau and amyloid were further confirmed by the comparison of tau SUVR and amyloid Centiloid,

where Type 3 showed significantly lower values than both Type 1 and Type 2, who, however, did not differ between each other (Fig. 2).

Voxel-wise brain hypometabolism and tau accumulation

Fig 3 shows the hypometabolism and tau patterns in the three subtypes. Type 1 showed significant cortical hypometabolism in the angular gyrus, precuneus, middle occipital gyrus, posterior cingulate cortex, supramarginal gyrus, middle temporal gyrus, and inferior temporal

Table 1. Demographic, clinical, and biomarker features of amnesic MCI subtypes: hippocampal-sparing with cortical hypometabolism subtype (Type 1), hippocampal and cortical hypometabolism subtype (Type 2) and medial temporal cortex hypometabolism (Type 3).

	Type 1 N = 27	Type 2 N = 23	Type 3 N = 22	p-Values
Age, y	72 ± 4.7	74 ± 5	74 ± 5.1	0.57
Sex, female %	53.3%	48.8%	31.8%	0.24
Education, y	14 ± 4.5	15 ± 3.2	16 ± 1.7	0.31
MMSE score at baseline	26 ± 2.6	26 ± 3.1	28 ± 1.7	0.01 ^a
MMSE score at follow-up	22 ± 5.1	24 ± 4	26 ± 2.7	0.001 ^a
MoCA score	20 ± 6.6	21 ± 3.5	24 ± 2.7	0.03 ^a
CDR	0.5 ± 0.2	0.5 ± 0	0.5 ± 0.2	0.576
RAVLT immediate recall	21 ± 13	23 ± 11	29 ± 14	0.15
RAVLT delay recall	7.9 ± 4.8	6 ± 5	8 ± 4.1	0.354
Amyloid status, positivity (+)	100%	100%	50%	0.02 ^a
Tau status, neocortex +	92%	100%	4%	<0.001 ^a
MTL +	/	/	18%	

Continuous variables are reported as mean ± standard deviation, categorical variables as percentages. *p*-Values are obtained by Kruskal–Wallis test for continuous variables and the proportion test for frequencies.

Abbreviations: CDR, clinical dementia rating; MMSE, mini-mental state examination; MOCA, montreal cognitive assessment; MTL, medial temporal lobes; N, number; RAVLT, rey auditory verbal learning test; y, year.

^aType 3 is significantly different from Types 1 and 2.

gyrus, when compared to the HC group. In this group, the tau pattern widely involved similar regions, such as medial and lateral temporal and parietal regions, including the precuneus and the posterior cingulate. Type 2 showed also cortical hypometabolism, however less extended, involving the left angular gyrus, left middle temporal gyrus, left superior temporal gyrus, posterior cingulate cortex, and precuneus. Of note, the medial temporal structures, particularly the hippocampus, were involved as well. Type 1 and Type 2 tau patterns were comparable, involving neocortical and medial temporal regions. Type 3 showed severe hypometabolism in the amygdala, hippocampus, and superior temporal gyrus, bilaterally. The tau pattern was negative at the group level, with a very limited uptake in the hippocampus driven by only a few cases (*N* = 4). Examples of individual cases are reported in Fig 1.

Of note, the direct comparison between Type 1 and Type 2 showed more severe hypometabolism in the inferior and superior parietal lobules (*p* < 0.001) in the former. Type 3 showed significantly lower hippocampal metabolism than Type 2 (*p* = 0.013).

In addition, Type 1 showed increased metabolism in the hippocampus than HC (*p* < 0.001). This group was the only one showing hippocampal hypermetabolism compared to the other two subtypes (*p* < 0.005).

The direct voxel-wise comparison of tau load between Type 1 and Type 2 showed no differences. In particular, although the hippocampus was not hypometabolic in Type 1, it had a comparable load of tau as Type 2 (*p* = 0.13).

Longitudinal cognitive trajectories among subtypes

Linear mixed effect models indicated that Type 1 (standardized β [stb] of interaction with time in years = −2.05, *p* < 0.001) has a faster decline over time on MMSE compared to Type 3 (reference) group (Fig. 4). Type 2 showed a flat slope in the range of follow-up time (2.3 ± 1.2).

Considering different tau status, we found that tau-positive individuals (stb = −1.2, *p* = 0.008) showed a faster cognitive decline over time compared to the tau-negative ones, independently from FDG-PET patterns (Fig. 4).

Discussion

MCI is a heterogeneous condition from the clinical and prognostic points of view.⁶ FDG-PET represents an established neurodegeneration biomarker able to reveal characteristic and progressive brain hypometabolism at the prodromal and preclinical neurodegenerative disease phases.^{25,26} This study describes three different aMCI subtypes based on FDG-PET hypometabolism patterns and tau deposition. Despite the comparable amnesic clinical phenotype at baseline, the brain metabolism subtypes differed in the tau accumulation, as assessed by PET, leading to different courses of cognitive decline over time. Type 1 and Type 2 showed extensive and comparable tau accumulation and clinical progression over time, with the former presenting the fastest cognitive decline (Fig. 4). On the contrary, Type 3 had no tau accumulation or was very limited to the MTL, and clinical stability, advocating for non-AD etiologies.² These findings underline the key role of the combination of brain metabolism and tau biomarkers for diagnosis and prognosis in aMCI. The present classification of individual FDG-PET patterns in prodromal aMCI confirms the existence of distinct hypometabolic subtypes, as previously shown in another aMCI cohort using FDG PET¹² or in AD dementia series using FDG-PET⁴ and MRI.³ However, there is still an ambiguous interpretation and consequent classification of the limbic-predominant pattern within the AD spectrum.^{3–5}

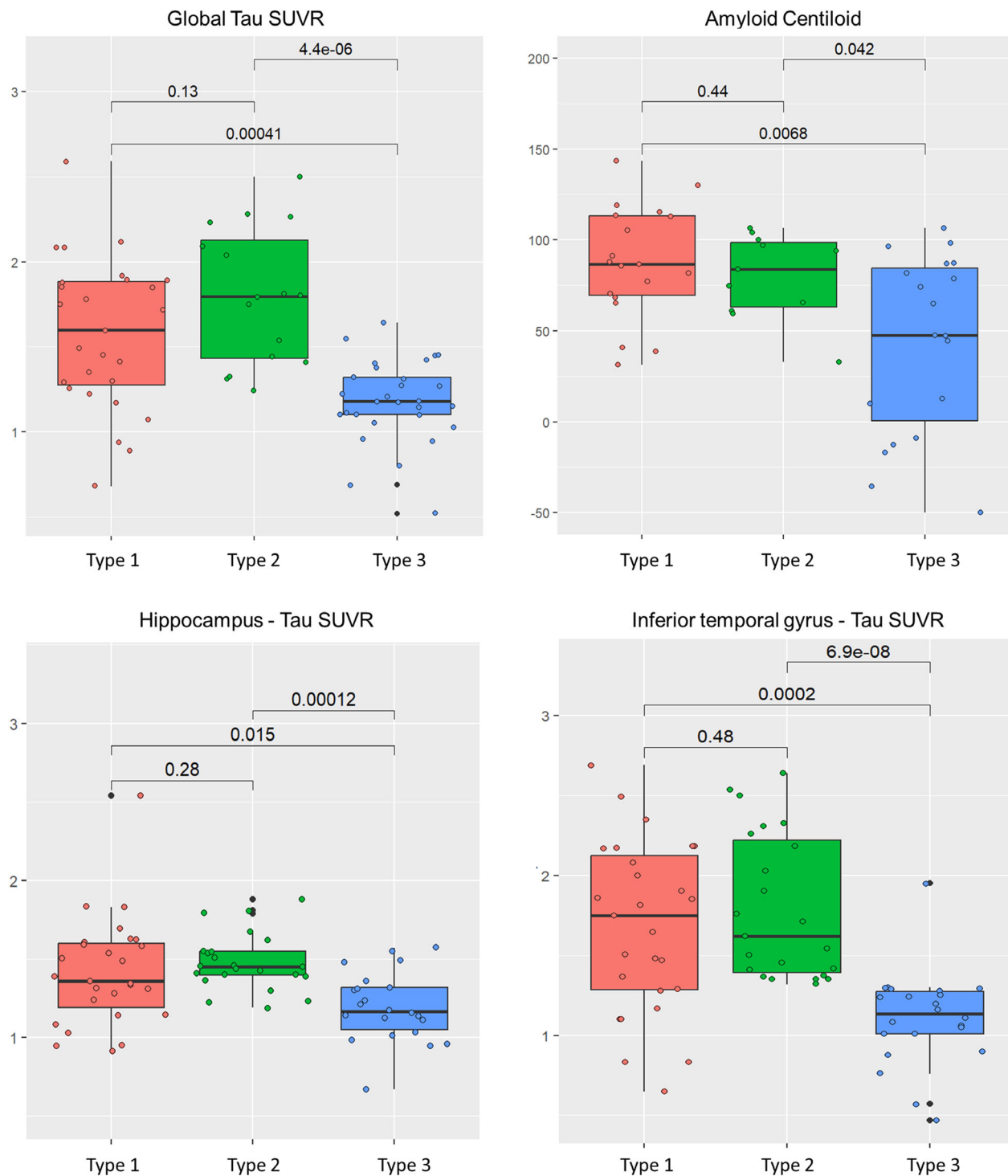


Figure 2. Amyloid and tau differences between subtypes. Boxplots show the distributions of tau SUVR and amyloid centiloids among FDG-based subtypes. The *p*-values, obtained from Kruskal–Wallis test with post hoc comparison, for each comparison are reported in the graphs. Type 1 corresponds to the hippocampal-sparing subtype with cortical hypometabolism; Type 2 to the typical AD subtype with hippocampal and cortical hypometabolism; Type 3 to the limbic subtype with medial temporal cortex hypometabolism.

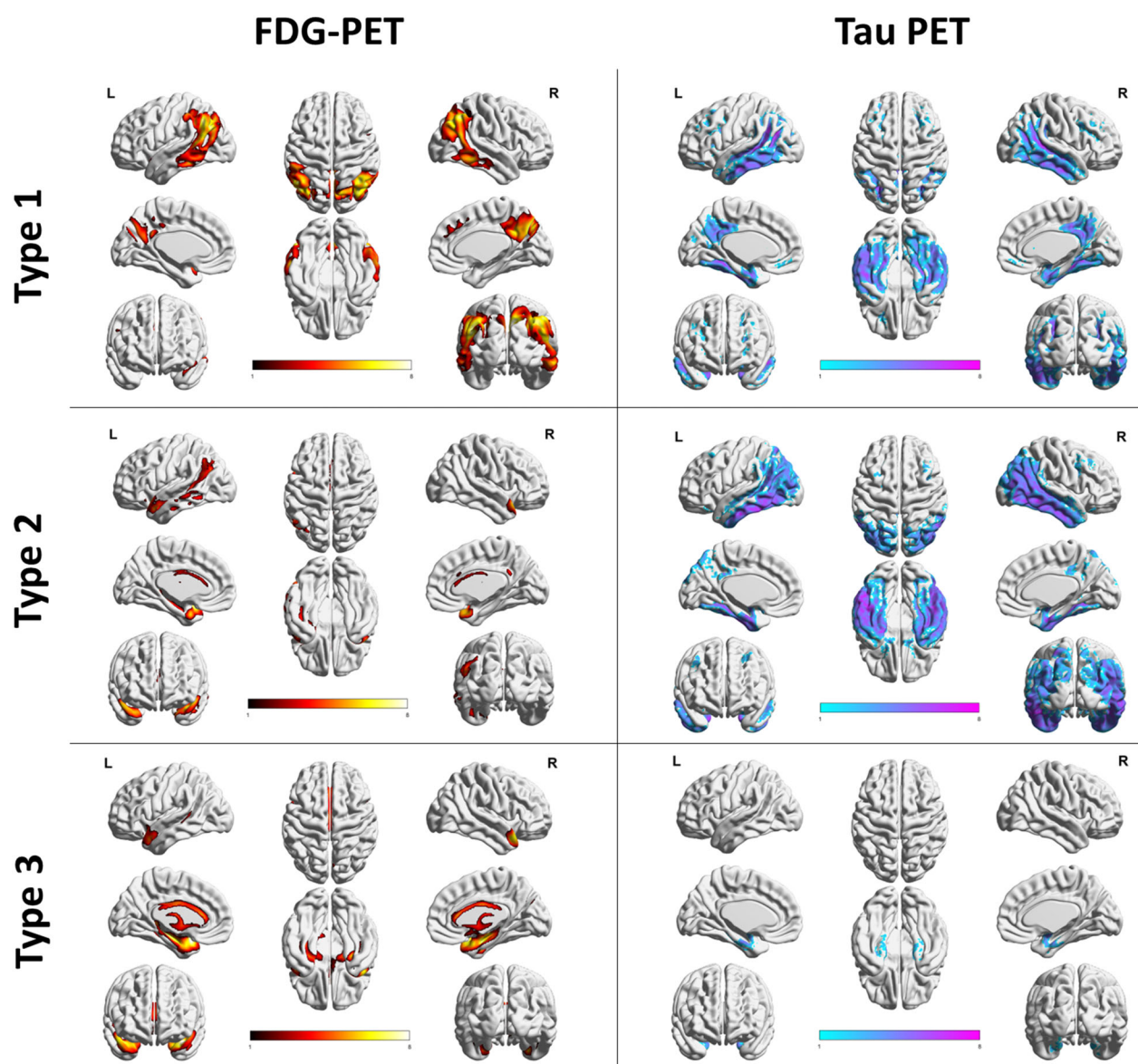


Figure 3. Topographical distribution of brain hypometabolism (FDG-PET) and tau load (tau-PET) at group level for each subtype. Topographical distributions of brain hypometabolism and tau load are obtained by SPM group analysis obtained by statistically comparing each group with healthy controls database (see text for details). Only brain regions showed significant differences from healthy controls are depicted yellow/red and light blue/pink color scales. Yellow/red and light blue/pink scales represent hypometabolism and tau load severity, respectively ($p < 0.05$, $k = 100$). Type 1 corresponds to the hippocampal-sparing subtype with cortical hypometabolism; Type 2 to the typical AD subtype with hippocampal and cortical hypometabolism; Type 3 to the limbic subtype with medial temporal cortex hypometabolism.

Here, we complemented with tau PET biomarker the specific hypometabolic patterns at the individual level in prodromal phase, contributing to patient's classification.

Type 1 represented 40% of our sample characterized by a posterior temporoparietal hypometabolism with sparing of hippocampal structures (Fig. 3). The hippocampal-sparing subtype in AD has been consistently proven,^{3–5,27} however, the mechanisms behind the vulnerability of the

associative cortices without involvement of the MTL are still unclear. In our prodromal sample, Type 1 was characterized by PET amyloid- and tau-positivity and a fast cognitive decline, thus representing the most malignant AD subtype. This finding is consistent with MRI studies in AD dementia patients which identified a malignant subtype characterized by great atrophy in the associative cortices and the worst cognitive progression^{3,5,27} and with

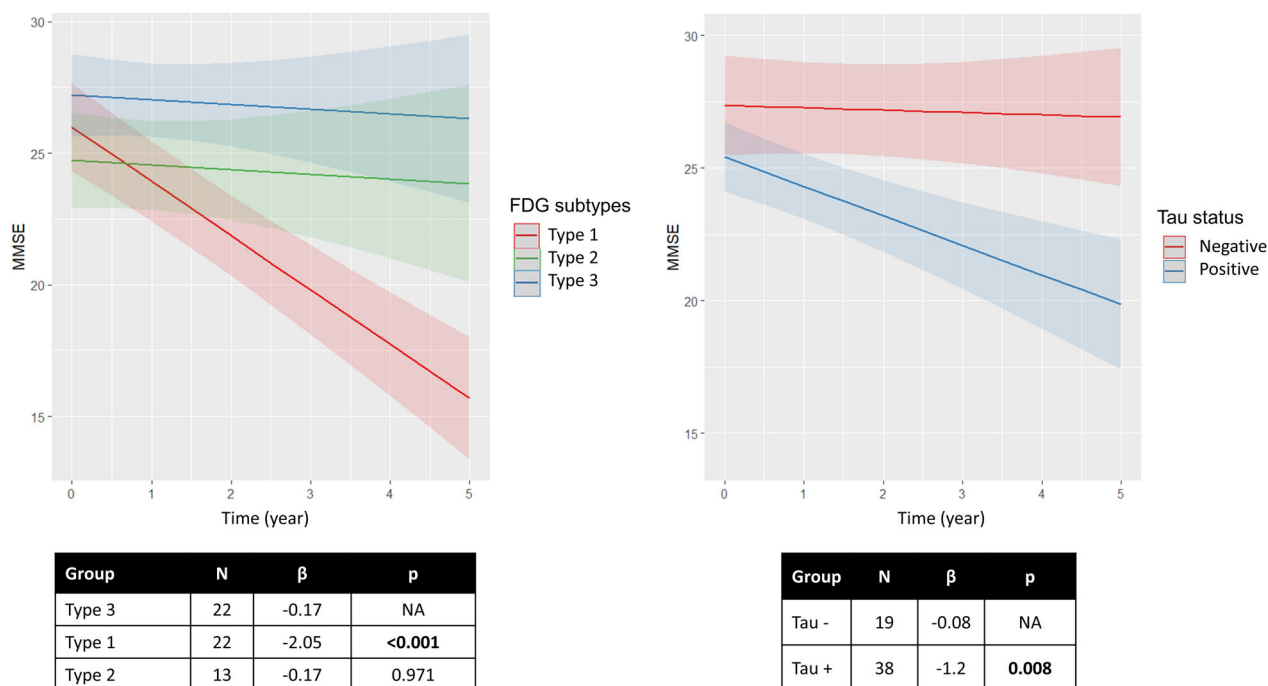


Figure 4. Longitudinal cognitive trajectories. The graph on the left shows different cognitive trajectories of MMSE scores over time in the different FDG-based subtypes. The graph on the right shows different cognitive trajectories of MMSE scores over time in tau-positive and -negative patients. Type 1 corresponds to the hippocampal-sparing subtype with cortical hypometabolism; Type 2 to the typical AD subtype with hippocampal and cortical hypometabolism; Type 3 to the limbic subtype with medial temporal cortex hypometabolism.

our previous FDG-PET study, showing a comparable hippocampal sparing subtype with high positivity of AD-CSF biomarkers and the highest level of cognitive decline and progression to AD dementia (73%).¹² Contrary to the clinical comparability of our subtypes, previous studies reported more commonly atypical AD non-amnesic presentations such as posterior cortical atrophy (PCA), logopenic primary progressive aphasia (LPPA), and the frontal variant of AD in hippocampal-sparing than in typical and limbic-predominant AD^{28,29} that can possibly explain the faster longitudinal cognitive decline in this subtype. Moreover, dysexecutive AD has been recently clinically described initially presenting as a progressive and predominant degradation of core executive functions in the absence of prominent behavioral features and, from the imaging side, patients usually report hypometabolism and tau deposition in posterior parietal cortices and variably in the frontal cortices with the MTL sparing in most patients.^{30,31}

Type 2, on the other hand, included 30% of the whole sample and showed the AD hypometabolic pattern in the medial temporal and temporoparietal cortices, however with less cortical involvement than Type 1 (Fig. 3). All Type 2 cases were amyloid- and tau-positive. Of note, Type 1 and 2 subtypes did not differ in amyloid and tau

accumulation loads (Fig. 2) and tau topographic pattern (Fig. 3). Tau pathology involved the MTL in both groups, although this structure was hypometabolic only in Type 2, whereas Type 1 showed relative hypermetabolism possibly reflecting the relatively spared metabolism of this structure. The concept of hippocampal-sparing subtype of AD could challenge the widely accepted model of NFT spreading from the entorhinal to the associative cortices.³² Instead, a less common pathway affecting first multimodal association cortices with a late limbic involvement can be advocated.³³ Of note, we found MTL relative hypermetabolism in Type 1 in the presence of tau pathology. A reported tau-associated hypermetabolism in temporal regions was suggested as an early sign of brain dysfunction associated with AD pathology.³⁴ The association between FDG-PET hypermetabolism and reduced memory performances has been also reported,^{35,36} as well as an association with a decrease of intrinsic connectivity between the hippocampus and precuneus.³⁷ Whether a hypermetabolic phase drives amyloidosis and/or tauopathy or is a consequence remains an open question. The most compelling hypothesis is that microglial responses follow the earliest amyloid fibrillization, leading to inflammatory glucose hypermetabolism and facilitating subsequent tau increases in early AD.³⁸ Thus, glucose

hypermetabolism can be associated with neuroinflammation in line with activated microglia consuming high levels of glucose.³⁸ Again, the hippocampal hypermetabolism was considered a detrimental rather than a beneficial compensatory reaction in cognitively impaired subjects.³⁵ Moreover, in MCI, soluble TREM2 as a measure of microglia activation was positively associated with hippocampal metabolism that was higher compared to healthy controls and able to predict conversion to dementia.³⁹ Our results also argued in favor of a detrimental effect of relative hypermetabolism in the hippocampus, possibly favoring tau deposition and fast spreading beyond the MTL, leading to a worse cognitive decline in Type 1 than other subtypes (Fig. 4).

Type 3 was the most benign subtype with significantly higher scores in global cognition at baseline (Table 1) and clinical stability over time (Fig. 4). This subtype showed a severe hypometabolism limited to the MTL structures. The presence of the amnesic phenotype with MTL hypometabolism has previously led to considering it as an AD limbic subtype.^{3,5} However, the limbic-predominant hypometabolic pattern showed a striking resemblance with the FDG-PET pattern of pathologically confirmed patients with MCI and dementia due to TDP-43 pathology and/or hippocampal sclerosis, as previously described.^{6,40} This specific pattern was able to distinguish the autopsy-confirmed cases with comorbid TDP-43 from AD.⁶ Moreover, a recent study reassessed the LATE-associated FDG-PET pattern in an independent autopsy cohort confirming its clinical utility in differentiating LATE and AD etiologies in dementia patients.⁴⁰ The importance of our study relies on the detection of this FDG-PET pattern plus the associated negative tau-PET scan in the prodromal MCI stage.

In our work, the possibility of non-AD pathological substrates was further supported by the clinically benign course over time in Type 3, in line with previous studies reporting a consistent rate of clinical stability (from 16% to 38%) in aMCI subjects with limbic-predominant hypometabolism.^{8,41} The absence of tau pathology as shown here, advocates non-AD conditions. Hippocampal sclerosis has been proposed as the main cause of memory loss in patients with stable aMCI and preservation of other cognitive functions,⁴² together with the primary age-related tauopathy (PART), which lacks pathological amyloid load,⁴³ and the LATE, with or without concomitant amyloid.² Despite the amyloid positivity in 50% of the cases, Type 3 had negative tau scans (78%) or very limited tau in hippocampal structure (18%) (according to current US Food and Drug Administration guidelines, the increased tracer uptake in MTL is considered nonsignificant for AD (negative scans)⁴⁴). We found only four cases with a minimal tau load in MTL, likely due to age-related

changes.^{45,46} The association between amyloid positivity and a diagnosis of AD dementia becomes weaker with aging,⁴⁷ and there is autopsy evidence for significant amyloid deposition in aged brains of people without antemortem dementia.⁴⁸ Concerning tau, our results fit with Botha *et al.* which demonstrated a negative tau-PET scan associated with a temporolimbic FDG-PET pattern in old amnesic subjects with autopsy-confirmed LATE pathology.⁶ A more recent study showed pathological suprathreshold values of p-tau181 in the CSF of patients with a LATE-like FDG-PET pattern.⁴⁰ However, CSF p-tau181 increases may not necessarily indicate NFT pathology.⁴⁹ Thus, the null or limited tau in Type 3 subjects hampers an AD etiology, that is instead strongly supported in both Type 1 and Type 2 by tau-PET uptake in medial and temporoparietal regions. A potential source of clinical challenges is the limbic AD variant, which localizes to the limbic system. In this scenario, the visual assessment of tau-PET can help in determining which pathology drives clinical symptoms. Thus, we further confirm that in the case of FDG-PET hypometabolism limited to limbic structures, a negative tau-PET would rule out an AD etiology.

Finally, when we split the sample into tau-positive and tau-negative subjects, tau status was able to discriminate between different cognitive trajectories supporting the key role of tau-PET in identifying stable or decliner subjects due to AD (Fig. 4).^{9,10} However, stratifying according to FDG-PET subtypes, we found a significantly steeper cognitive decline of Type 1 compared to other subtypes (Fig. 4). The cognitive decline of Type 2 was less malignant than Type 1 (Fig. 4), possibly because of a less severe cortical hypometabolism in these individuals (Fig. 3) and/or also the limited follow-up durations. Other factors such as brain resilience, cognitive reserve, and compensation could contribute to explaining the cognitive trajectories in Type 2 that might decline later.⁵⁰ The steeper progression to dementia associated with the Type 1 hypometabolic pattern highlights the potential of FDG-PET to identify a more malignant subtype with more severe neurodegeneration likely due to the combination of other drivers. Our results highlight the importance of establishing tau positivity in participants with amnesic phenotype and neurodegeneration to confirm that their neurodegeneration is due to AD.¹¹ The ability of tau-PET in identifying aMCI subjects with a malignant or benign course has undeniable prognostic and therapeutic repercussions since the design of clinical trials should include proper AD cases and avoid enrolling individuals who will not develop AD dementia.

The novelty of this study is the demonstration of how tau assessed by PET differs in FDG-defined aMCI subtypes, supporting AD and non-AD diagnosis and

predicting fast cognitive decline. More importantly, in the development of disease-modifying therapies, tau-PET has a potential role in the accurate selection of AD patients that will benefit most from already-developed drugs and tau-targeting therapeutics. Moreover, as tau-PET is not largely available, FDG-PET, as a more widely accessible technique, can also help to identify AD cases and the more malignant subtype among them. Notably, recent advancements have demonstrated that FDG-PET scans contain sufficient data to allow for the accurate synthesis of tau-PET scans through artificial intelligence⁵¹ and they also harbor additional crucial data for diagnosing and understanding a broader range of neurodegenerative disorders beyond AD, such as frontotemporal dementia (FTD) and dementia with Lewy bodies (DLB).⁵²

Among the limitations, we acknowledge a relatively small sample size that was longitudinally evaluated with a short follow-up period. Second, we are aware that no absolute consensus on the cutoff point for amyloid status definition is to date available but we applied here a threshold previously validated.^{10,23} Lastly, the main limitation of our study is the lack of postmortem examination, which hampers a conclusive etiology explanation. Nevertheless, our findings imply major clinical remarks for diagnosis and prognosis given that the limbic hypometabolism pattern is quite frequent in the aMCI population corresponding to 30% of the present and previous analyzed samples,^{8,11} and separating the non-AD limbic cases is of utmost importance. Longitudinal imaging studies will provide further insight into the evolution of the different subtypes.

Author Contributions

D.P. was responsible for the study concept and design. C.B. and S.P.C. were responsible for all neuroimaging analyses and statistical analyses. C.B. was responsible for drafting the original report which was reviewed and revised by all coauthors (S.P.C., A.C., G.B.F., D.P., and V.G.). V.G. was responsible for the acquisition of the PET scan at HUG. G.B.F. was responsible for the acquisition of the clinical data at HUG. All authors were responsible for the interpretation of data for the work.

Acknowledgments

The Memory Centre is funded by the following private donors under the supervision of the Private Foundation of Geneva University Hospitals: A.P.R.A. – Association Suisse pour la Recherche sur la Maladie d'Alzheimer, Genève; Fondation Segré, Genève; Race Against Dementia Foundation, London, UK; Fondation Child Care, Genève;

Fondation Edmond J. Safra, Genève; Fondation Minkoff, Genève; Fondazione Augusta, Lugano; McCall Macbain Foundation, Canada; Nicole et René Keller, Genève; Fondation AETAS, Genève. The Clinical Research Centre, at Geneva University Hospital and Faculty of Medicine provides valuable support for regulatory submissions and data management, and the Biobank at Geneva University Hospital for biofluid processing and storage. We thank the Centre for Radiopharmaceutical Sciences of ETH and USZ for providing the PET tracer for tau imaging. Avid radiopharmaceuticals provided access to the [¹⁸F] flortaucipir radiotracer but were not involved in data analysis or interpretation. Data used in preparation of this article were obtained from the Alzheimer's Disease Neuroimaging Initiative (ADNI) database (adni.loni.usc.edu). As such, the investigators within the ADNI contributed to the design and implementation of ADNI and/or provided data but did not participate in analysis or writing of this report. A complete listing of ADNI investigators can be found at: http://adni.loni.usc.edu/wp-content/uploads/how_to_apply/ADNI_Acknowledgement_List.pdf. Data collection and sharing for this project was also funded by the AD Neuroimaging Initiative (ADNI) (National Institutes of Health Grant U01 AG024904) and DOD ADNI (Department of Defense award number W81XWH-12-2-0012). ADNI is funded by the National Institute on Aging, the National Institute of Biomedical Imaging and Bioengineering, and through generous contributions from the following: AbbVie, Alzheimer's Association; Alzheimer's Drug Discovery Foundation; Araclon Biotech; BioClinica, Inc.; Biogen; Bristol-Myers Squibb Company; CereSpir, Inc.; Cogstate; Eisai Inc.; Elan Pharmaceuticals, Inc.; Eli Lilly and Company; EuroImmun; F. Hoffmann-La Roche Ltd and its affiliated company Genentech, Inc.; Fujirebio; GE Healthcare; IXICO Ltd.; Janssen Alzheimer Immunotherapy Research & Development, LLC.; Johnson & Johnson Pharmaceutical Research & Development LLC.; Lumosity; Lundbeck; Merck & Co., Inc.; Meso Scale Diagnostics, LLC.; NeuroRx Research; Neurotrack Technologies; Novartis Pharmaceuticals Corporation; Pfizer Inc.; Piramal Imaging; Servier; Takeda Pharmaceutical Company; and Transition Therapeutics. The Canadian Institutes of Health Research is providing funds to support ADNI clinical sites in Canada. Private sector contributions are facilitated by the Foundation for the National Institutes of Health (www.fnih.org). The grantee organization is the Northern California Institute for Research and Education, and the study is coordinated by the Alzheimer's Therapeutic Research Institute at the University of Southern California. ADNI data are disseminated by the Laboratory for Neuro Imaging at the University of Southern California.

Funding Information

Competitive research projects have been funded by: H2020 (projects n. 667375), Innovative Medicines Initiative (IMI contract n. 115736 and 115952), IMI2, Swiss National Science Foundation (projects n. 320030_182772 and n. 320030_169876), VELUX Foundation. VG was supported by the Swiss National Science Foundation (projects 320030_169876, 320030_185028 and IZSEZO_188355), by the Velux Foundation (project 1123), by the Schmidheiny Foundation, the Boninchi Foundation and by the Aetas Foundation.

Conflict of Interest

VG received research support and speaker fees through her institution from GE Healthcare, Siemens Healthineers, Novo Nordisk and Janssen. GBF has received support, payment, consulting fees or honoraria for lectures, presentations, speakers bureaus, manuscript writing, or educational events from: Biogen, Roche, Diadem, Novo Nordisk, GE HealthCare, OM Pharma, and Eisai (all through his institution). AC reports speaker honoraria from General Electric Healthcare, Novartis, Sirtex, Blue Earth Diagnostics, AmGen. Consulting fees from Blue Earth Diagnostics, Novartis. The other authors have no conflicts of interest pertinent to this manuscript.

References

- Petersen RC, Roberts RO, Knopman DS, et al. Mild cognitive impairment: ten years later. *Arch Neurol*. 2009;66(12):1447-1455.
- Nelson PT, Dickson DW, Trojanowski JQ, et al. Limbic-predominant age-related TDP-43 encephalopathy (LATE): consensus working group report. *Brain*. 2019;142(6):1503-1527.
- Ferreira D, Nordberg A, Westman E. Biological subtypes of Alzheimer disease: a systematic review and meta-analysis. *Neurology*. 2020;94(10):436-448.
- Levin F, Ferreira D, Lange C, et al. Data-driven FDG-PET subtypes of Alzheimer's disease-related neurodegeneration. *Alzheimers Res Ther*. 2021;9:1-14.
- Ossenkoppele R, Lyoo CH, Sudre CH, et al. Distinct tau PET patterns in atrophy-defined subtypes of Alzheimer's disease. *Alzheimers Dement*. 2020;16(2):335-344. doi:10.1016/j.jalz.2019.08.201
- Botha H, Mantyh WG, Murray ME, et al. FDG-PET in tau-negative amnesic dementia resembles that of autopsy-proven hippocampal sclerosis. *Brain*. 2018;141(4):1201-1217.
- Mohanty R, Ferreira D, Frerich S, et al. Neuropathologic features of antemortem atrophy-based subtypes of Alzheimer disease. *Neurology*. 2022;99(4):E323-E333.
- Tondo G, Carli G, Santangelo R, et al. Biomarker-based stability in limbic-predominant amnesic mild cognitive impairment. *Eur J Neurol*. 2021;28:1123-1133.
- Ossenkoppele R, Smith R, Mattsson-Carlgren N, et al. Accuracy of tau positron emission tomography as a prognostic marker in preclinical and prodromal Alzheimer disease: a head-to-head comparison against amyloid positron emission tomography and magnetic resonance imaging. *JAMA Neurol*. 2021;78:961.
- Boccalini C, Ribaldi F, Hristovska I, et al. The impact of tau deposition and hypometabolism on cognitive impairment and longitudinal cognitive decline. *Alzheimers Dement*. 2023;20:221-233.
- Botha H, Mantyh WG, Graff-Radford J, et al. Tau-negative amnesic dementia masquerading as Alzheimer disease dementia. *Neurology*. 2018;90(11):e940-e946.
- Caminiti SP, De Francesco S, Tondo G, et al. FDG-PET markers of heterogeneity and different risk of progression in amnesic MCI. *Alzheimers Dement*. 2024;20:159-172.
- Perani D, Anthony P, Rosa D, et al. Validation of an optimized SPM procedure for FDG-PET in dementia diagnosis in a clinical setting. *Neuroimage Clin*. 2014;6:445-454.
- Guedj E, Varrone A, Boellaard R, et al. EANM procedure guidelines for brain PET imaging using [¹⁸F] FDG, version 3. *Eur J Nucl Med Mol Imaging*. 2021;49:632-651. doi:10.1007/s00259-021-05603-w
- Caminiti SP, Sala A, Presotto L, et al. Validation of FDG-PET datasets of normal controls for the extraction of SPM-based brain metabolism maps. *Eur J Nucl Med Mol Imaging*. 2021;48:2486-2499.
- Della Rosa PA, Cerami C, Gallivanone F, et al. A standardized [¹⁸F]-FDG-PET template for spatial normalization in statistical parametric mapping of dementia. *Neuroinformatics*. 2014;12(4):575-593.
- Presotto L, Ballarini T, Caminiti SP, Bettinardi V, Gianolli L, Perani D. Validation of ¹⁸F-FDG-PET single-subject optimized SPM procedure with different PET scanners. *Neuroinformatics*. 2017;15(2):151-163.
- Fleisher AS, Pontecorvo MJ, Devous MD, et al. Positron emission tomography imaging with [¹⁸F] flortaucipir and postmortem assessment of Alzheimer disease neuropathologic changes. *JAMA Neurol*. 2020;77:829-839.
- Mathoux G, Boccalini C, Peretti DE, et al. A comparison of visual assessment and semi-quantification for the diagnostic and prognostic use of [¹⁸F] flortaucipir PET in a memory clinic cohort. *Eur J Nucl Med Mol Imaging*. 2024;1-12. doi:10.1007/s00259-023-06583-9
- Rolls ET, Huang CC, Lin CP, et al. Automated anatomical labelling atlas 3. *NeuroImage*. 2020;206:116189. doi:10.1016/j.neuroimage.2019.116189
- Mishra S, Gordon BA, Su Y, et al. AV-1451 PET imaging of tau pathology in preclinical Alzheimer disease: defining a summary measure. *NeuroImage*. 2017;161:171-178.

22. Klunk WE, Koeppe RA, Price JC, et al. The centiloid project: standardizing quantitative amyloid plaque estimation by PET. *Alzheimers Dement*. 2015;11(1):1-15.
23. Jack CR, Wiste HJ, Weigand SD, et al. Defining imaging biomarker cut points for brain aging and Alzheimer's disease. *Alzheimers Dement*. 2017;13(3):205-216. doi:10.1016/j.jalz.2016.08.005
24. Tzourio-Mazoyer N, Landeau B, Papathanassiou D, et al. Automated anatomical labeling of activations in SPM using a macroscopic anatomical parcellation of the MNI MRI single-subject brain. *NeuroImage*. 2002;15(1):273-289.
25. Perani D, Caminiti SP, Carli G, Tondo G. PET neuroimaging in dementia conditions. *PET SPECT Neurology*. 2nd ed. 2020. doi:10.1007/978-3-030-53168-3
26. Minoshima S, Cross D, Thientunyakit T, Foster NL, Drzezga A. ¹⁸F-FDG PET imaging in neurodegenerative dementing disorders: insights into subtype classification, emerging disease categories, and mixed dementia with copathologies. *J Nucl Med*. 2022;63(6):2S-12S.
27. Murray ME, Graff-Radford NR, Ross OA, Petersen RC, Duara R, Dickson DW. Neuropathologically defined subtypes of Alzheimer's disease with distinct clinical characteristics: a retrospective study. *Lancet Neurol*. 2011;10(9):785-796. doi:10.1016/S1474-4422(11)70156-9
28. Ferreira D, Mohanty R, Murray ME, Nordberg A, Kantarci K, Westman E. The hippocampal sparing subtype of Alzheimer's disease assessed in neuropathology and in vivo tau positron emission tomography: a systematic review. *Acta Neuropathol Commun*. 2022;10(1):1-19. doi:10.1186/s40478-022-01471-z
29. Graff-Radford J, Yong KXX, Apostolova LG, et al. New insights into atypical Alzheimer's disease in the era of biomarkers. *Lancet Neurol*. 2021;20(3):222-234.
30. Townley RA, Graff-Radford J, Mantyh WG, et al. Progressive dysexecutive syndrome due to Alzheimer's disease: a description of 55 cases and comparison to other phenotypes. *Brain Commun*. 2020;2(1):1-19.
31. Corriveau-Lecavalier N, Barnard LR, Lee J, et al. Deciphering the clinico-radiological heterogeneity of dysexecutive Alzheimer's disease. *Cereb Cortex*. 2023;33(11):7026-7043.
32. Braak H, Alafuzoff I, Arzberger T, Kretschmar H, del Tredici K. Staging of Alzheimer disease-associated neurofibrillary pathology using paraffin sections and immunocytochemistry. *Acta Neuropathol*. 2006;112(4):389-404.
33. Ferreira D, Mohanty R, Murray ME, Nordberg AK, Kantarci K, Westman E. Does a truly hippocampal sparing subtype of Alzheimer's disease really exist? *Alzheimers Dement*. 2021;17(S4):1-2.
34. Hanseeuw BJ, Betensky RA, Schultz AP, et al. Fluorodeoxyglucose metabolism associated with tau-amyloid interaction predicts memory decline. *Ann Neurol*. 2017;81(4):583-596.
35. Apostolova I, Lange C, Mäurer A, et al. Hypermetabolism in the hippocampal formation of cognitively impaired patients indicates detrimental maladaptation. *Neurobiol Aging*. 2018;65:41-50.
36. Rubinski A, Franzmeier N, Neitzel J, Ewers M. FDG-PET hypermetabolism is associated with higher tau-PET in mild cognitive impairment at low amyloid-PET levels. *Alzheimers Res Ther*. 2020;12(1):1-12.
37. Tahmasian M, Pasquini L, Scherr M, et al. The lower hippocampus global connectivity, the higher its local metabolism in Alzheimer disease. *Neurology*. 2015;84(19):1956-1963.
38. Biel D, Suárez-Calvet M, Hager P, et al. sTREM2 is associated with amyloid-related p-tau increases and glucose hypermetabolism in Alzheimer's disease. *EMBO Mol Med*. 2023;15(2):1-13.
39. Choi H, Choi Y, Lee EJ, et al. Hippocampal glucose uptake as a surrogate of metabolic change of microglia in Alzheimer's disease. *J Neuroinflammation*. 2021;18(1):1-15.
40. Grothe MJ, Moscoso A, Silva-Rodríguez J, et al. Differential diagnosis of amnesic dementia patients based on an FDG-PET signature of autopsy-confirmed LATE-NC. *Alzheimers Dement*. 2023;19:1234-1244.
41. Cerami C, Dodich A, Iannaccone S, et al. A biomarker study in long-lasting amnesic mild cognitive impairment. *Alzheimers Res Ther*. 2018;10(1):42.
42. Bien CG, Helmstaedter C, Elger CE. Is it really Alzheimer's disease? *J Neurol Neurosurg Psychiatry*. 2001;71:416-417.
43. Teylan M, Mock C, Gauthreaux K, et al. Cognitive trajectory in mild cognitive impairment due to primary age-related tauopathy. *Brain*. 2020;143(2):611-621.
44. Mattay VS, Fotenos AF, Ganley CJ, Marzella L. Brain tau imaging: food and drug administration approval of ¹⁸F-flortaucipir injection. *J Nucl Med*. 2020;61(10):1411-1412.
45. Wuestefeld A, Pichet Binette A, Berron D, et al. Age-related and amyloid-beta-independent tau deposition and its downstream effects. *Brain*. 2023;146:awad135.
46. Costoya-Sánchez A, Moscoso A, Silva-Rodríguez J, et al. Increased medial temporal tau positron emission tomography uptake in the absence of amyloid-β positivity. *JAMA Neurol*. 2023;80(10):1051-1061.
47. Iaccarino L, Sala A, Perani D. Predicting long-term clinical stability in amyloid-positive subjects by FDG-PET. *Ann Clin Transl Neurol*. 2019;6(6):1113-1120.
48. Elobeid A, Libard S, Leino M, Popova SN, Alafuzoff I. Altered proteins in the aging brain. *J Neuropathol Exp Neurol*. 2016;75(4):316-325.

49. Moscoso A, Grothe MJ, Ashton NJ, et al. Time course of phosphorylated-tau181 in blood across the Alzheimer's disease spectrum. *Brain*. 2021;144(1):325-339.
50. Neuner SM, Telpoukhovskaia M, Menon V, O'Connell KMS, Hohman TJ, Kaczorowski CC. Translational approaches to understanding resilience to Alzheimer's disease. *Trends Neurosci*. 2022;45(5):369-383. doi:[10.1016/j.tins.2022.02.005](https://doi.org/10.1016/j.tins.2022.02.005)
51. Lee J, Burkett BJ, Min H, et al. Synthesizing images of tau pathology from cross-modal neuroimaging using deep learning. *bioRxiv*. 2022.
52. Jones D, Lowe V, Graff-Radford J, et al. A computational model of neurodegeneration in Alzheimer's disease. *Nat Commun*. 2022;13(1):1643.